Detailed Population Balance Modelling of TiO_2 Synthesis in an Industrial Reactor

Astrid Boje[a], Jethro Akroyd[a], Stephen Sutcliffe[c], John Edwards[c], Markus Kraft[a,b,*]

[a] *Department of Chemical Engineering and Biotechnology, University of Cambridge, New Museums Site, Pembroke Street, Cambridge, CB2 3RA, United Kingdom*
[b] *School of Chemical and Biomedical Engineering, Nanyang Technological University, 62 Nanyang Drive, Singapore, 637459*
[c] *Huntsman Pigments and Additives, Titanium House, Hanzard Drive, Wynyard Park, TS22 5FD, United Kingdom*

Abstract

This paper uses a network of ideal flow reactors and a detailed population balance model to study the evolution of the size and shape distributions of pigmentary titanium dioxide, formed under industrial synthesis conditions. The industrial reactor has multiple reactant injections, a tubular working zone in which the exothermic reaction is completed, and a cooling zone. A network of continuously stirred tank reactors is used to model variation in composition around the feeds and plug flow reactors with prescribed temperature gradients are used to describe the working and cooling zones. The quality of the industrial product depends on its morphology, and this is influenced by factors including temperature and throughput. In this paper, a multivariate particle model is accommodated using a stochastic method and the particle morphology is characterized in terms of the distributions of primary and aggregate particle diameters, number of primary particles per particle and neck radii of connected primary particles. Increasing temperature or residence time is shown to produce larger particles. Qualitative similarities are highlighted between such findings and previous studies. The throughput studies are also in qualitative agreement with empirical industrial experience. There is scope for extending and improv-

*Markus Kraft
Email address: mk306@cam.ac.uk (Markus Kraft)

ing the current model; however, it is suggested that insights of this type could be used to inform the design and operation of the industrial process.

Keywords: titanium dioxide, ideal reactor, network, particle model, stochastic, population balance

1. Introduction

Titanium dioxide (TiO_2, titania) powder is used ubiquitously in pigments, as well as in cosmetics, pharmaceuticals, ceramics and catalysts. It can be synthesised by the oxidation of titanium tetrachloride ($TiCl_4$) in either a flame, or by stage-wise addition to a plasma (Akroyd et al., 2011; Gázquez et al., 2014). The TiO_2-forming reaction has the overall stoichiometry:

$$TiCl_4 + O_2 \rightarrow TiO_{2(\text{particles})} + 2Cl_2.$$

The optical properties of the product are determined by the particle size and morphology. For example, the tint depends on the particle size distribution (PSD); and the crystal phase determines the magnitude of the refractive index and the photocatalytic nature of the product (Chen and Mao, 2007; Kartaev et al., 2014; West et al., 2007). The use of this reaction in titanium dioxide pigment manufacture necessitates milling of the particles to achieve the necessary size and distribution for light scattering. Milling has a significant impact on the energy cost of the product; thus, ease of milling can be an important consideration.

Many factors influence the size and morphology of the particles, including the gas-phase reaction rates, particle processes, operating conditions, type of plasma-forming gas, reactor configuration and use of chemical additives. Park and Park (2015) discuss the role of these different factors and summarise the difficulties inherent in understanding and controlling the synthesis process.

Reactors for the industrial synthesis of titanium dioxide often have multiple feed points, with independently controlled feed rates and pre-heat temperatures (West et al., 2007). The operating conditions include temperatures in the range

1000-1500 K, pressures of up to 4.5 bara and residence times in the milliseconds. This limits the availability of industrially relevant studies; thus most published experimental work is under milder laboratory-scale and flame synthesis conditions. Laboratory-scale synthesis in different plasmas at atmospheric pressure was investigated by Kartaev et al. (2014); and Garrick and Wang (2011); George et al. (1973); Hong et al. (2005) and Tsantilis et al. (2002) have considered particle growth in a flame reactors.

These studies are important – for example, the thin film studies of Ghoshtagore (1970) and the hot wall reactor of Pratsinis et al. (1990) have provided insights into the kinetics of the overall oxidation reaction. However, the rates of the particle growth processes are significantly different under industrial conditions. For instance, a study by Pratsinis and Spicer (1998) found that the surface growth rate was significantly higher at high $TiCl_4$ concentrations. In the absence of published experimental data for the industrial synthesis of titanium dioxide, it is useful to compare the available literature to numerical studies under the elevated temperatures and pressures used in the industrial process. The model discussed in this paper aims to facilitate this objective.

Numerical studies of titania synthesis generally involve a population balance model that accounts for processes such as nucleation, coagulation, surface reaction and sintering. A concise review of the processes and common numerical methods can be found in Kraft (2005). This model is typically solved using monodisperse (Koch and Friedlander, 1990; Kruis et al., 1993; Pratsinis and Spicer, 1998; Spicer et al., 2002), moment (Akroyd et al., 2011; Frenklach and Harris, 1987), sectional (Tsantilis and Pratsinis, 2000; Xiong and Pratsinis, 1991, 1993) or finite element (Artelt et al., 2006) methods. These techniques are popular because they provide a set of differential equations for the particle dynamics that can be solved with the chemistry and flow. However, the limitation of these methods is that they require the description of each particle to remain relatively simple. Particles are typically spherical and are only described by a measure of their size, or of their size and volume.

The treatment of the particle processes is constrained by the level of detail

inherent in the particle model. For example, in a spherical model, collisions must result in perfect coalescence (Pratsinis and Spicer, 1998). Menz and Kraft (2013) found that incorporating more detail about the particles was particularly important for cases where coagulation and sintering occur on similar time scales, or where the coagulating particles are highly polydisperse.

Stochastic methods can be used to extend to multivariate particle type spaces. They allow efficient tracking of an arbitrary number of particle properties for a fully polydisperse population by considering particle processes as discrete events that occur on computational particles in a representative sample volume. Aggregate structure can thus be resolved by explicitly tracking properties such as the number of connected primary particles, the shared surface area and the extent of sintering between primaries for each computational particle.

Stochastic population balance modelling has been used to simulate formation of soot (Celnik et al., 2007), silica (Shekar et al., 2012) and titania (Akhtar et al., 1994; West et al., 2007). Yapp et al. (2016) used a detailed population balance to compute the optical band gap of polycyclic aromatic hydrocarbons in an ethylene diffusion flame. Menz et al. (2014) used a stochastic method to investigate the synthesis of silicon nanoparticles, using a network of ideal reactors to describe flow behaviour in the reactor.

In this work, a stochastic method is used to resolve fully the particle structure beyond the extent that is possible using monodisperse, bidisperse, moment or sectional methods. This information is believed to be important here because particle structure directly relates to the optical properties of the final product, and the energy requirement of the milling step in the industrial process.

Computational fluid dynamics (CFD) simulations have been used to model the flow fields in titania synthesis in laboratory-scale plasma-chemical reactors (Kartaev et al., 2014, 2015), flame reactors (Mehta et al., 2010; Xu et al., 2016) and industrially representative reactors (Akroyd et al., 2011). The non-ideal flow patterns observed in the reactor cases suggest that treatment of flow is an important consideration for a model of the industrial system. For example, Kartaev et al. (2015) showed mixing in a recirculation zone induced by the

injection of quench gas by eight perpendicular jets into the mainstream, and Akroyd et al. (2011) illustrated circulation in the velocity field near the reactant injection site, with axial flow in the direction of the mainstream further downstream. However, the computational cost of solving the flow with CFD limits the complexity of the chemistry and particle models that can be used.

The equivalent reactor network (ERN) approach couples ideal reactors, such as continuously stirred tank reactors (CSTRs) and plug flow reactors (PFRs), to approximate the flow behaviour observed experimentally or by CFD. This has been used to simplify the treatment of turbulent reacting flows in models for particle synthesis so that an acceptable level of detail can be obtained in the chemistry and particle models (Novosselov et al., 2006; Novosselov and Malte, 2008; Mehta et al., 2010, 2013). Treatment of turbulent reacting flows has also been approached using stochastic reactor models (SRMs) such as the partially stirred plug flow reactor (PaSPFR), for example for a carbon black furnace Balthasar et al. (2002).

The **purpose of this paper** is to demonstrate the potential to simulate the synthesis of TiO_2 in an industrial reactor, using a detailed population balance model to obtain information about particle properties, such as size and morphology, which determine the product quality. Coupling to CFD on a realistic reactor geometry (especially with many perpendicular feed jets at multiple feed points) is out of scope at present, due to the complexity of the chemistry and particle model in the current principle study. Thus, a network of ideal reactors is employed to account for variation in composition, temperature, and localised mixing. A linear network of CSTRs and PFRs is used to model an industrial reactor. The model is also applied to investigate different process conditions, which could be useful for predicting the effect of process phenomena such as temperature hot-spots on the product properties.

The **structure of this paper** is as follows: Section 2 discusses the particle model and processes, and gives a brief overview of the numerical methods used. Section 3 introduces the reactor network model and the base case operating conditions. Section 4.1 presents the results of the base case simulation and dis-

cusses related numerical considerations. Section 4.2 presents a short sensitivity study for reactor temperature, configuration and throughput, mentioning relevant literature studies and industrial experience. Finally, the current work is summarised in Section 5, along with suggestions for future work.

2. Model and methods

This work uses coupled solvers for the gas-phase chemistry and particle population balance. The chemical mechanism proposed by West et al. (2009) is used for the gas-phase. It includes 28 gas-phase species, one solid species and 66 gas-phase reactions. A multivariate particle model is used and the population balance, which describes the formation and growth of particulate titania, is solved using a stochastic method.

2.1. Particle model

The simulation system is comprised of computational particles P_i, with $i = 1, \ldots, N \leq N^{(\max)}$, in a sample volume V_{smp} (**Fig. 1**). Each computational particle represents a certain number of physical particles and the sample volume defines the scaling between the physical system and the simulated system. The user-defined upper limit on the number of computational particles in the simulation is given by $N^{(\max)}$.

Each particle P_i is an aggregate structure which is described by a list of its n_i constituent primary particles p_j, $j = 1, \ldots, n_i$. Information about the connectivity between the primary particles is also stored (Menz and Kraft, 2013; Yapp et al., 2016) such that P_i is defined by:

$$P_i = (p_1, \ldots, p_{n_i}, \mathbf{C}) \,.$$

Here, $\mathbf{C}$ represents the structure that stores the connectivity, degree of sintering and shared surface area data for each pair of neighbouring primary particles in P_i. For a detailed explanation of the implementation of $\mathbf{C}$, see Sander et al.

(2009) and Shekar et al. (2012). Each primary particle p_j is defined in terms of the number, $\eta \in \mathbb{N}_0$, of titanium, oxygen and chlorine atoms it contains:

$$p_j = (\eta_{\mathrm{Ti}}, \eta_{\mathrm{O}}, \eta_{\mathrm{Cl}})\,.$$

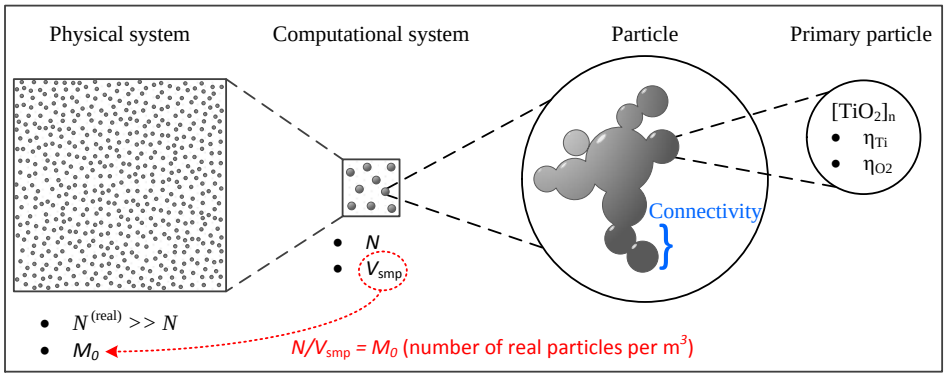

Fig. 1. Computational representation of the physical system, using N simulation particles in a sample volume V_{smp}, and primary particle connectivity and composition within the particle.

The primary particle volume $v\,(p_j)$ is computed from its composition:

$$v\,(p_j) = \frac{1}{N_{\mathrm{A}}} \sum_{k=1}^{N_{\mathrm{components}}} \frac{\eta_k W_k}{\rho_k}, \tag{1}$$

where W_k refers to the molecular weight of component k, ρ_k is its mass density and N_{A} is Avogadro's constant. The primary diameter, d_{p}, and area, a_{p}, are computed by:

$$d_{\mathrm{p}}\,(p_j) = \left(\frac{6v\,(p_j)}{\pi}\right)^{\frac{1}{3}}, \tag{2}$$

$$a_{\mathrm{p}}\,(p_j) = \pi(d_{\mathrm{p}}\,(p_j))^2. \tag{3}$$

The collision diameter, d_{c}, of each particle is computed from the total particle volume, V_i, and area, A_i, as in Eq. (4), assuming a fractal dimension of 1.8 as

discussed in Sander et al. (2009) and Tsantilis et al. (2002). V_i and A_i are calculated by summation of the particle's primary particle volumes and surface areas, adjusted for the effect of sintering (see Section 2.2.4).

$$d_{\mathrm{c}}\left(P_i\right) = \frac{6V_i}{A_i} n_i{}^{\frac{1}{1.8}} \tag{4}$$

Constant/variable fractal dimensions are studied in Goudeli et al. (2015). Expressions for the collision diameter are compared by Patterson and Kraft (2007). It has been suggested that the specific choice for approximating aggregate structure does not have a significant effect relative to the current understanding of the formation and growth processes (Patterson and Kraft, 2007; Tsantilis et al., 2002).

Theoretical convergence of the population balance equation as $N^{(\max)} \to \infty$ has been studied by Eibeck and Wagner (2003); Patterson (2013, 2016) and Wells (2006).

2.2. Particle processes

The formation and growth processes in the population balance model include inception, surface growth, coagulation and sintering (**Fig. 2**).

The whole aggregate structure is available due to use of the multivariate particle model. For each stochastic particle, the list of its primary particles (with their individual compositions), the primary particle connectivity, the degree of sintering and the shared surface area between each pair of neighbouring primary particles is tracked throughout the simulation. Each stochastic particle is an aggregate consisting of one or many primary particles; thus, the different processes can be defined in terms of properties such as surface area, collision diameter or mass of the primary/aggregate particles, since these properties can be derived from the tracked information. The processes act on (pairs of) primary particles or whole particle aggregates as highlighted in Sections 2.2.1-2.2.4.

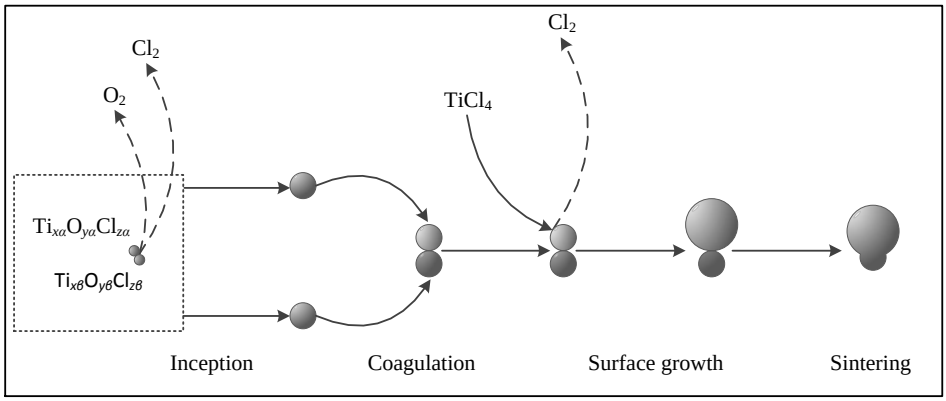

Fig. 2. Particle formation and growth processes for titania.

2.2.1. Inception

Inception refers to the nucleation of primary particles from precursor gas-phase species. Here, possible particle inception reactions are defined by a set of 105 bimolecular collisions between the various titanium oxychloride species ($\mathrm{Ti}_x\mathrm{O}_y\mathrm{Cl}_z$, $x, y, z \geq 1$) that are generated by the gas-phase mechanism, and the collision rate is determined by a transition regime coagulation kernel, with a molecular collision diameter of 0.65 nm (Akroyd et al., 2011; Celnik et al., 2007; Sander et al., 2009; West et al., 2007). The inception reactions have the form:

$$\mathrm{Ti}_{x_\alpha}\mathrm{O}_{y_\alpha}\mathrm{Cl}_{z_\alpha} + \mathrm{Ti}_{x_\beta}\mathrm{O}_{y_\beta}\mathrm{Cl}_{z_\beta} \rightarrow (x_\alpha + x_\beta)\,\mathrm{TiO}_{2\,(\mathrm{s})} + \left(\frac{y_\alpha + y_\beta}{2} - x_\alpha - x_\beta\right)\mathrm{O}_2 + \left(\frac{z_\alpha + z_\beta}{2}\right)\mathrm{Cl}_2.$$

2.2.2. Surface reaction

Primary particles undergo growth due to surface reaction with gaseous species. Here, the heterogeneous surface reaction is assumed to be first order in TiCl_4 and O_2, as in Akroyd et al. (2011). The growth rate is given by Eq. (5), where k_s has Arrhenius form as in Eq. (6), and A refers to the surface area per unit

volume of the particle population. Values for the parameters k_1 and E_a were obtained by fitting the data from the experiment of Pratsinis et al. (1990): $k_1 = 1.34 \times 10^3$ m/s·m^3/mol and $E_a = 60$ kJ/mol.

$$\frac{d\left[\mathrm{TiO_2}\right]}{dt} = k_s A \left[\mathrm{TiCl_4}\right]\left[\mathrm{O_2}\right] \tag{5}$$

$$k_s = k_1 \exp\left(-\frac{E_a}{RT}\right) \ \frac{\mathrm{m}}{\mathrm{s}} \cdot \frac{\mathrm{m}^3}{\mathrm{mol}} \tag{6}$$

It is not currently possible to validate these values at the higher end of the temperature range pertinent to this work (ca 1300-1500 K) owing to the absence of relevant surface rate data. However, the Arrhenius form is still expected to be suitable in this range and, at present, there is no evidence to suggest a different reaction mechanism at elevated temperatures.

2.2.3. Coagulation

Coagulation between particles P_i and P_j involves collision and lasting point contact, and is governed by the Smoluchowski equation (Eibeck and Wagner, 2001). The rate is described by the transition regime coagulation kernel K_{tr}, which is calculated as half the harmonic mean of the slip flow and free molecular kernels, K_{sf} and K_{fm} as in Eqs. (7)-(9), in which m is the particle mass, k_B is the Boltzmann constant, P is the pressure, and Kn is given by Eq. (10) (Shekar et al., 2012).

$$K_{tr} = \frac{K_{sf} K_{fm}}{K_{sf} + K_{fm}} \tag{7}$$

$$K_{sf}\left(P_i, P_j\right) = \frac{2k_B T}{3\mu}\left(\frac{1 + 1.257\mathrm{Kn}\left(P_i\right)}{d_c\left(P_i\right)} + \frac{1 + 1.257\mathrm{Kn}\left(P_j\right)}{d_c\left(P_j\right)}\right)\left(d_c\left(P_i\right) + d_c\left(P_j\right)\right) \tag{8}$$

$$K_{fm}\left(P_i, P_j\right) = 2.2\sqrt{\frac{\pi k_B T}{2}\left(\frac{1}{m\left(P_i\right)} + \frac{1}{m\left(P_j\right)}\right)}\left(d_c\left(P_i\right) + d_c\left(P_j\right)\right)^2 \tag{9}$$

$$\mathrm{Kn}\left(P_i\right) = 4.74 \times 10^{-8} \frac{T}{P d_{\mathrm{c}}\left(P_i\right)} \tag{10}$$

2.2.4. Sintering

Particle rounding occurs due to sintering; which is modelled between neighbouring pairs of primary particles p_i and p_j. As in other work (West et al., 2007; Xiong and Pratsinis, 1993), it is assumed that the excess radius over that of a mass-equivalent spherical particle decays exponentially. Thus, the change in the common particle surface area, $A_{i,j}$, due to sintering is given by Eq. (11), in which $A_{i,j}^{\mathrm{sph}}$ is the surface area of a mass-equivalent spherical particle.

$$\frac{dA_{i,j}}{dt} = -\frac{1}{\tau_{\mathrm{c}}}\left(A_{i,j} - A_{i,j}^{\mathrm{sph}}\right) \tag{11}$$

The characteristic sintering time, τ_{c}, is given by Eq. (12), in which $d_{i,j}$ is the minimum diameter of the two primaries. The expression was proposed by Kobata et al. (1991) and derives from TiO_2 particles sintering through grain-boundary diffusion. This approach was used by West et al. (2007). Alternate expressions for τ_{c} are available (Park and Park, 2015).

$$\tau_{\mathrm{c}} = 7.4 \times 10^{8} T d_{i,j}^{4} \exp\left(\frac{3.1 \times 10^{4}}{T}\right) \tag{12}$$

The sintering level $s_{i,j}$ between the primary particle pairs in each particle is given by Eq. (13), as in Shekar et al. (2012). This describes the extent to which sintering has occurred; $s_{i,j} = 0$ implies that the particles are in point contact and $s_{i,j} \geq 0.95$ implies that the primaries have coalesced to form a new particle (Yapp et al., 2016). Intermediate levels, $s_{i,j} \in (0, 0.95)$, describe partially sintered particles, connected by a 'neck' of non-zero radius, and ability to describe such connections is believed to be one of the advantages of a multivariate particle model. The sintering level is tracked for each pair p_i, p_j in all particles P_i.

$$s_{i,j} = \frac{\frac{A_{i,j}^{\mathrm{sph}}}{A_{i,j}} - 2^{-1/3}}{1 - 2^{-1/3}} \tag{13}$$

2.3. Numerical methods

The coupling between the gas-phase and particle systems is treated using an operator-splitting technique (Celnik et al., 2007). The gas-phase reactions are handled using an ordinary differential equation solver and the population balance can be solved using either a direct simulation algorithm (DSA) or a stochastic weighted algorithm (SWA) (Patterson et al., 2011; Shekar et al., 2012). The DSA was used for the simulations in this work. The reactors in the network are solved sequentially (Menz et al., 2014). See Appendix B for the algorithms.

In the population balance solver, inflow, inception, coagulation and surface growth are modelled as stochastic processes and outflow and sintering are modelled as continuous processes. Continuous outflow is used to minimise propagation of error, as recommended by Menz et al. (2014), and is achieved by rescaling the sample volume. The waiting time between events is assumed to be exponentially distributed and the mean of the distribution is specified by the overall process rate for the current state. The probability of selecting a particular process is given by the ratio of the individual and overall process rates.

The DSA assigns equal statistical weights to each computational particle in the ensemble. That is, each computational particle represents the same number of physical particles. This means that coagulation events deplete the sample, because each event combines two of the computational particles. In SWA, particles are given unequal weights. When a coagulation occurs, one of the two particles involved is left unaltered, and the other particle is updated to have the properties of the particle that would result from the coagulation event. This is accounted for by changing the weight of the updated particle as described elsewhere (Patterson et al., 2011). This improves the resolution of rare/large particles and can be useful for variance reduction in systems in which coagulation occurs to a large extent.

In order to improve computational efficiency, a linear process deferment algorithm (Patterson et al., 2006) is implemented for surface growth. A majorant

technique (Eibeck and Wagner, 2000; Patterson et al., 2011) is used to compute the coagulation rate and perform coagulation events efficiently. A binary tree data structure is used to store the particle lists, providing an efficient means of selecting particles based on a specific property (Patterson et al., 2006).

3. Reactor model

The specific industrially representative titania reactor considered in this work has two distinct zones (**Fig. 3**). High temperature oxygen enters the dosing zone (the shaded part) at $x = 0$, and $TiCl_4$ and O_2 gas is fed through the wall at three subsequent points. The second part of the reactor is called the working zone. Here, the gas-phase reactions continue to completion and the particulate product undergoes further growth. A qualitative temperature profile is shown in the lower half of Fig. 3. The temperature does not increase significantly in the dosing zone due to the effect of reactant injections through the reactor wall. The temperature increases across the working zone due to the exothermic oxidation reaction. The particulate product from the reactor is then cooled in a cooler that is several times the reactor length.

An ideal reactor network (**Fig. 4**) is used to account for the axial variation in composition and temperature, while keeping the flow model simple enough to use a detailed particle model. This consists of a linear sequence of eleven CSTRs and two PFRs.

The CSTRs are used as a dynamic model of the reactor dosing zone because good mixing is assumed to occur near the dosing points. We note that this assumption forms the basis of the current ERN study. Although a realistic CFD study is presently out of range, particularly in conjunction with the detailed particle model used in this work, it would be useful to investigate the flow behaviour in more detail at a later stage to validate this assumption for the industrial reactor.

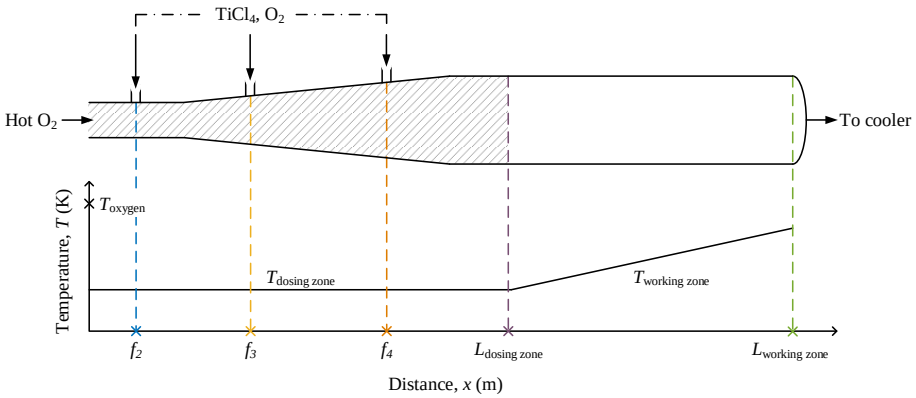

Fig. 3. Schematic of industrial titania reactor showing rough axial temperature profile and location of each feed stage relative to the reactor length L, $L = L_{\text{dosing zone}} + L_{\text{working zone}}$ (not to scale). The labels f_2, f_3, f_4 designate the feed points.

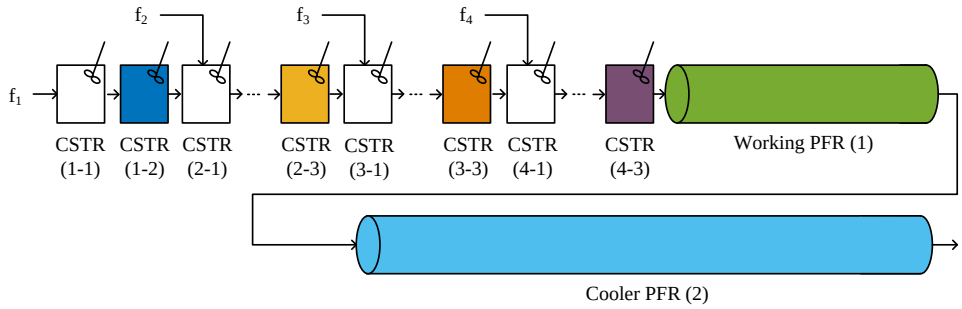

Fig. 4. Reactor network with feed f_i to CSTR (i-1), i.e. the first reactor in the i^{th} section, $i = 1, \ldots, 4$. Results will be shown for CSTRs (1-2), (2-3), (3-3), (4-3) and PFRs (1) and (2).

Fresh $TiCl_4$ and O_2 is injected to every third CSTR in the network, as shown in Fig. 4. The injection streams have volumetric feed fractions f_2, f_3 and f_4 relative to the total volumetric inflow to the corresponding reactor. PFRs with prescribed positive and negative temperature gradients are used to model the reactor working zone and the cooler respectively. Conditions are given in **Table 1**.

Typical industrial conditions are used, such as an approximately equimolar ratio of $TiCl_4$ to O_2 in feeds f_2, f_3 and f_4 (Akroyd et al., 2011) and a pressure of around 4 bara. Feed f_1 is predominantly O_2 with a small amount of $TiCl_4$.

Table 1. Base case operating conditions where D/W/C are the dosing/working/cooling zones.

Zone	Reactor	Feed fraction	Residence time	Temperature
-	-	f	τ, ms	T, K
D	CSTR (1-1)	1.0	2.0	1200
D	CSTR (1-2)	0	2.0	1200
D	CSTR (2-1)	0.50	5.0	1200
D	CSTR (2-2)	0	5.0	1200
D	CSTR (2-3)	0	5.0	1200
D	CSTR (3-1)	0.30	5.0	1200
D	CSTR (3-2)	0	5.0	1200
D	CSTR (3-3)	0	5.0	1200
D	CSTR (4-1)	0.40	5.0	1200
D	CSTR (4-2)	0	5.0	1200
D	CSTR (4-3)	0	5.0	1200
W	PFR (1)	0	160	1200-1600
C	PFR (2)	0	1500	1600-400

4. Results and discussion

The reactor network model is used to study the distributions of the size and structural characteristics of titania particles formed under industrial synthesis conditions. Particle growth is investigated in detail for a base case simulation in Section 4.1, with a brief discussion of numerical considerations in Section 4.1.2. In Section 4.2, a parameter study is used to compare the product size and structure resulting from different process conditions.

4.1. Base case

The evolution of the particle distributions under the base case conditions is shown in **Fig. 5**. The characteristics chosen for study are the number of primaries per particle (Fig. 5(a)), the mean collision and primary diameters (Figs. 5(b) and 5(c)) and the mean neck radius (Fig. 5(d)) for each aggregate. The mean value and the densities derived from a kernel estimator are included with the distributions to highlight the trends across the reactor-cooler.

The Matlab *ksdensity* function (MathWorks, 2016) was used to fit the estimates based on a normal kernel function for the discrete simulation data, using the default adaptive bandwidth, and the fits were normalised to illustrate the number density. The fourth sub-figure in each case compares the kernel estimators at the end of the reactor and cooler respectively.

The neck radius is computed by solving the difference between the common surface area and volume, and the surface area and volume of a pair of mass equivalent spheres, for the distance between the particle centres as described and illustrated in Lindberg et al. (2016).

Inception dominates near the beginning of the reactor due to the high reactant concentration and lack of particle surface area for surface reaction. Thus, most aggregates consist of one/several small primary particles and have small collision diameters (Fig. 5, CSTR (1-2)). The small mean neck radius indicates that most aggregated particles are only in point contact. Further down the dosing zone, the distributions become increasingly broad as the particles become more polydisperse and more significantly connected (Fig. 5, CSTR (4-3)).

Coagulation increases the mean collision diameters and number of primary particles of the particles. Surface growth increases the primary diameters and the neck radii become larger due to sintering between neighbouring primaries. Because coagulation is fast relative to sintering under the base case conditions, a significant proportion of the particles remains in point contact across the reactor (e.g. Fig. 5(d), CSTR (4-3)).

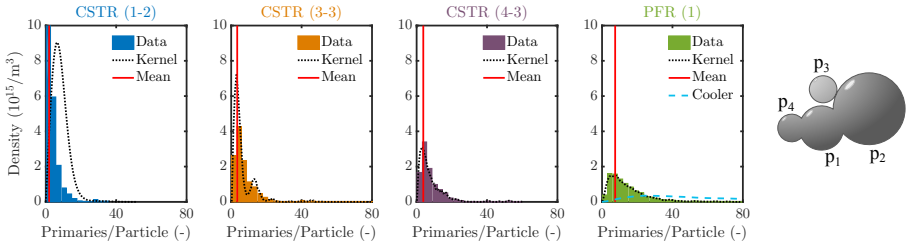

(a) Number of primaries per particle

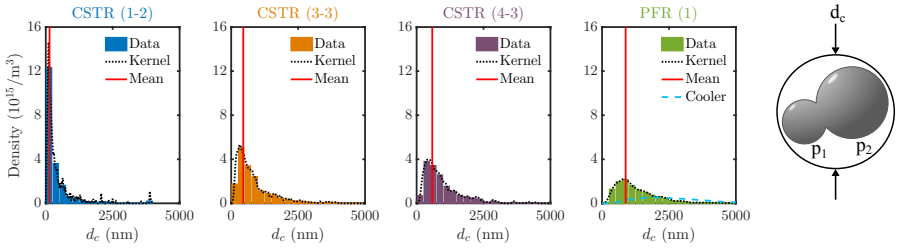

(b) Collision diameter, d_c

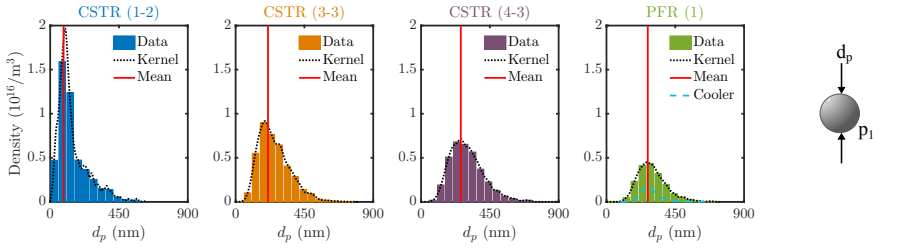

(c) Primary diameter, d_p

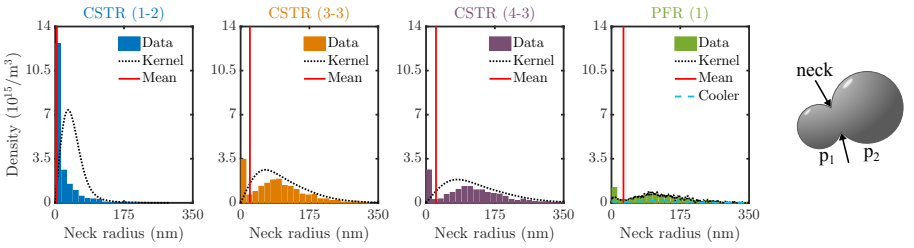

(d) Neck radius

Fig. 5. Raw simulation data, kernel density estimate and mean of the PSD in CSTRs (1-2), (3-3), (4-3) and PFR (1); and kernel density estimate for PFR (2). Right-hand schematics illustrate each property.

In the working zone and cooler, the gas-phase precursor is depleted and there is no further substantial change in mean primary diameter (Fig. 5(c), PFR (1)). Coagulation and sintering continue, producing increasingly broad, flat distributions with large mean collision and neck diameters (Figs. 5(a),5(b), 5(d) PFR (1)). Further primary growth could occur by complete sintering of neighbouring particles since merging changes the primary composition (cf. Eqs. (1)-(2)); however, this contribution was not significant in the current simulation.

4.1.1. Transient evolution of particle properties

The transient evolution of the particle collision diameters is explored at times 0.05τ, 0.5τ, τ and 5τ (τ = 2 ms) in CSTR (1-1). Lognormal kernel density estimates (Appendix A) for the collision diameter raw data are compared in **Fig. 6**. At the early time, the distribution consists of a single peak, that is just larger than the incepting particle size (0.49 nm). For 0.5τ and τ, the mean of the distribution is increasingly large due to coagulation (increasing the particle collision diameter) and surface growth (indirectly contributing to a larger collision diameter by increasing the primary diameters).

The absence of a peak at the incepting particle size (0.49 nm) suggests that coagulation is rapid, especially for the smallest particles. By 5τ, the steady-state has been established and this is observed to consist of a bimodal distribution, with a peak centred at the incepting particle size and a second peak at approximately 550 nm. These observations indicate that the characteristic time of the coagulation process is relatively short compared to the CSTR residence time.

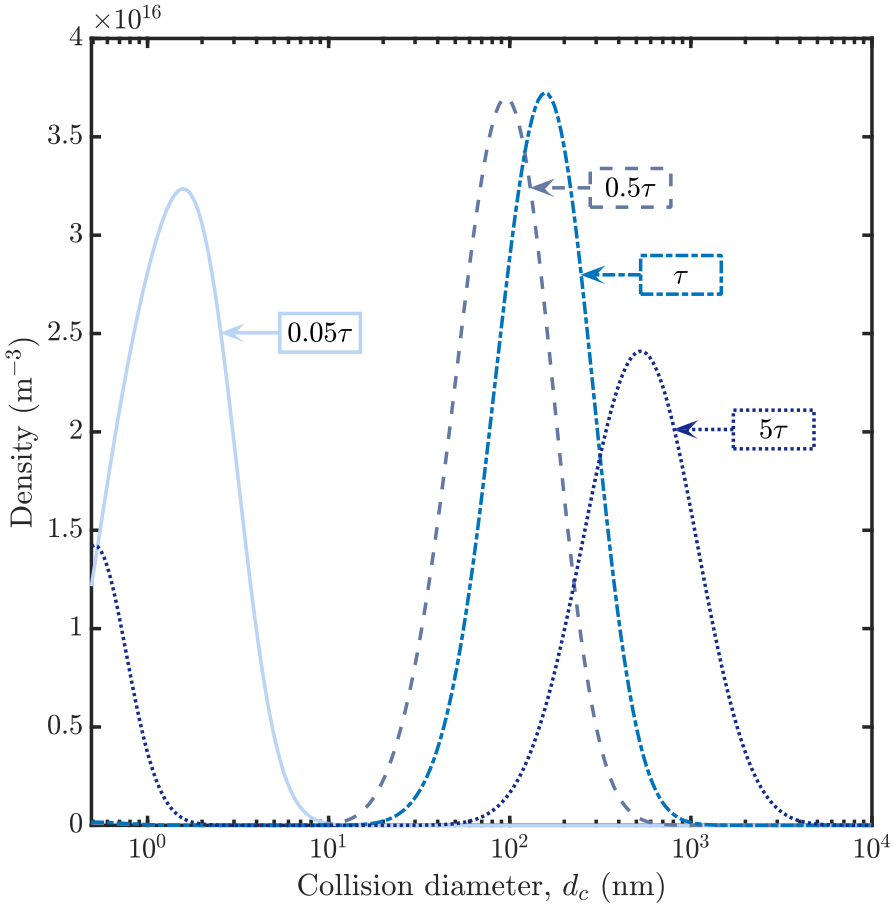

Fig. 6. Lognormal kernel estimates (with $\sigma = 0.4$) for the collision diameter simulation data, for four time points during transience in CSTR (1-1) with $\tau = 2$ ms. Extension below 0.49 nm is a consequence of the continuous smoothing kernel.

4.1.2. Numerical considerations

The direct simulation algorithm was used to produce the results presented in this paper. The stochastic weighted algorithm was found to produce comparable statistical errors across the network. However, in contrast to a previous study for CSTR networks with recycles (Menz et al., 2014), SWA was not found to reduce the statistical error in the particle moments. This is because the current

reactor network is linear. The run time with 2^{14} particles was approximately 33 hours (for DSA) on a 3 GHz Intel Xeon X5472 processor with 8 GB of RAM, running 64-bit CentOS Linux 7.

The statistical error and convergence behaviour are shown for CSTR (2-1), under the base case simulation conditions, using DSA. The average relative statistical error, $\bar{\epsilon}_{\text{stat}}$, is defined in Eq. (14), where M is the number of time steps included in the calculation, N and R are the ensemble capacity and the number of repeats, and c_θ and μ_θ are the 99.9% confidence interval and the mean for the property θ (Menz et al., 2014).

$$\bar{\epsilon}_{\theta,\text{stat}} = \frac{1}{M} \sum_{m=1}^{M} \frac{c_\theta^{(N,R)}(t_m)}{\mu_\theta^{(N,R)}(t_m)} \tag{14}$$

The particle mass moments are used as defined in Eq. (15), where, w_i is the statistical weight of the i^{th} particle (corresponding to the relative number of physical particles it represents) and ρ is the mass density of TiO_2. For DSA, all particles have the same statistical weight (here $w_i = 1$).

$$M_k(t) = \frac{1}{V_{\text{smp}}} \sum_{i=1}^{N(t)} w_i (\rho V_i)^k, \quad k = 0, 1, 2 \tag{15}$$

The statistical errors in the lower order particle moments, the collision diameter, the primary diameter and the number of primary particles per particle (n_{p}) are compared using $N^{(\max)} = 2^{14}$ computational (aggregate) particles and $R = 10$ repeat runs (**Fig. 7**). The statistical errors are observed to increase in the higher order moments as was found in other works (Menz et al., 2014; Patterson et al., 2011). The statistical errors in properties that are of interest in this work are sufficiently low.

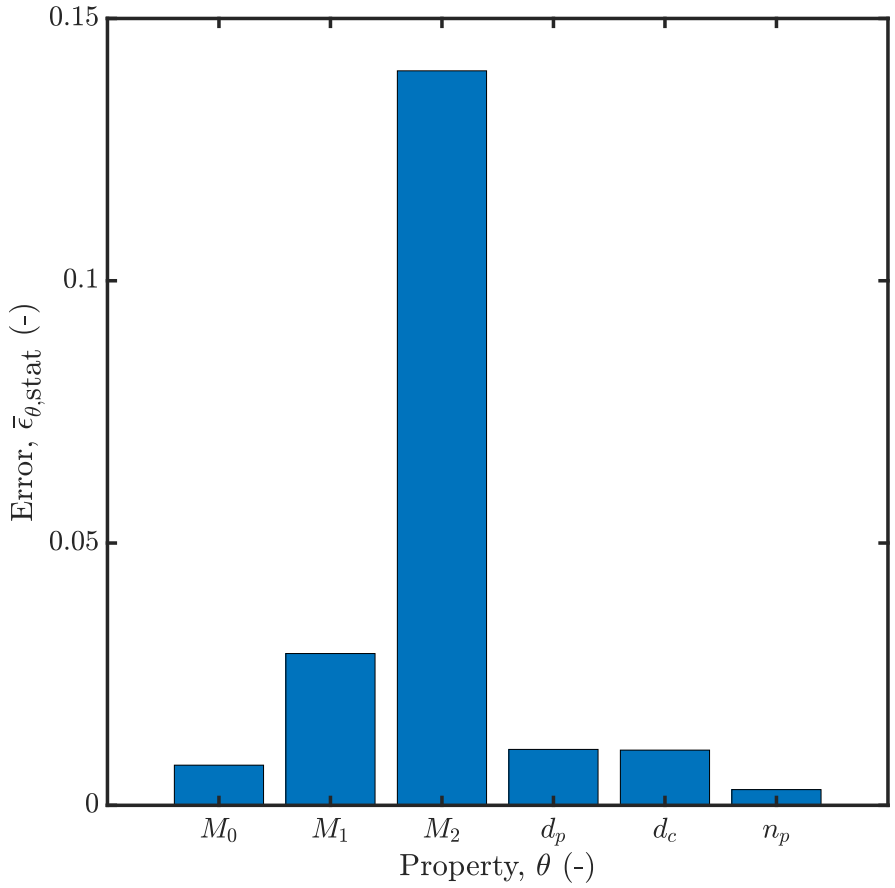

Fig. 7. Steady-state statistical error of the particle moments and the particle size characteristics in CSTR (2-1).

Convergence as a function of the number of computational particles is shown for the particle and primary particle diameters and the first mass moment with $N^{(\max)} \times R = 2^{17}$ (**Fig. 8**). All properties are relatively level by $N^{(\max)} = 2^{14}$, the value used elsewhere in this work.

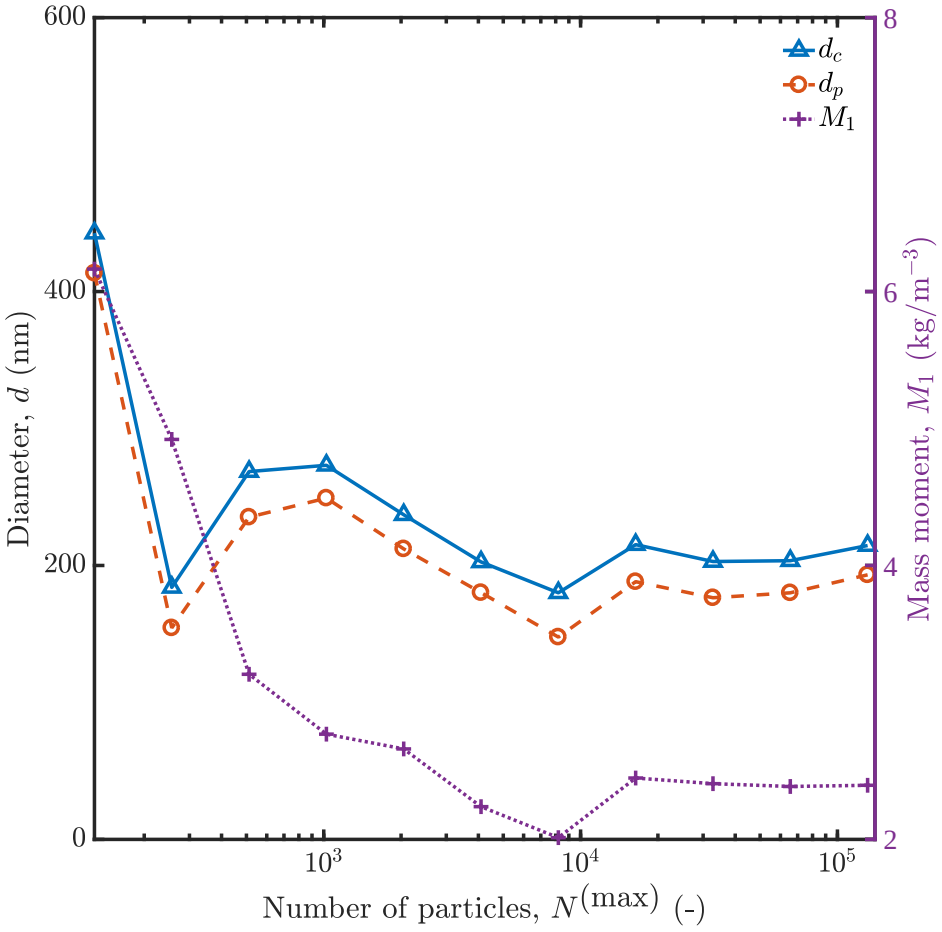

Fig. 8. Steady-state convergence behaviour of the particle moments and the particle size characteristics in CSTR (2-1).

4.2. Preliminary sensitivity study

The effect of changing configuration and operating conditions on the particle properties is explored to demonstrate the potential to use the detailed model to understand the process and important parameters. Three reactor configurations (test cases 0, 1 and 2), two temperatures (test cases 0 and 3) and two residence times (test cases 0 and 4) were considered, as summarised in **Table 2**. The

configuration was varied by moving the location of the three feed sites (**Fig. 9**).

The effect of temperature and residence time on the particle size and structure is summarised using the mean and geometric standard deviation of the aggregate and primary particle diameters, the number of primaries per particle and the number density (**Fig. 10** and **Table 3**). These properties are chosen so as to accommodate qualitative comparison with literature studies and plant experience, in the absence of relevant data.

Table 2. Operational parameters used in the base case (0) and test cases (1-4) varying the feed injection points, temperature and flow rate. $\{\tau\}_{\mathrm{bc}}$ is the set of base case residence times.

Case	Temperature	2^{nd} feed	3^{rd} feed	4^{th} feed	Residence time
-	T, K	CSTR #	CSTR #	CSTR #	$\{\tau\}$, ms
0	1200	3	6	9	$1 \times \{\tau\}_{\mathrm{bc}}$
1	1200	2	3	4	$1 \times \{\tau\}_{\mathrm{bc}}$
2	1200	9	10	11	$1 \times \{\tau\}_{\mathrm{bc}}$
3	1100	3	6	9	$1 \times \{\tau\}_{\mathrm{bc}}$
4	1200	3	6	9	$\frac{1}{2} \times \{\tau\}_{\mathrm{bc}}$

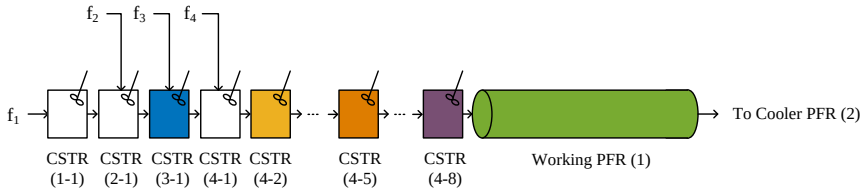

(a) Early dosage injection inlets (case 2)

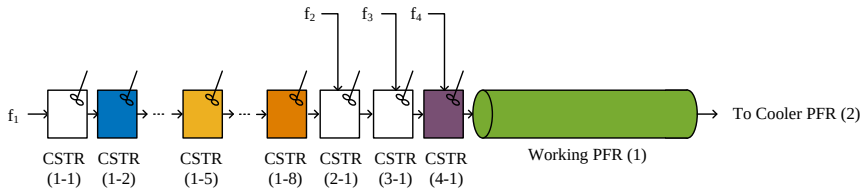

(b) Late dosage injection inlets (case 3)

Fig. 9. Reactor network configurations with different dosing points compared to the base case reactor dosing scheme, in which f_2, f_3 and f_4 were allocated to the third, sixth and ninth CSTRs respectively.

In the base case, particle inception dominates near the reactor inlet, as can be seen from the preliminary spike in the number density in Fig. 10. The surface reaction proceeds rapidly across the dosing zone, near the fresh feed points, and a sharp increase in the mean primary diameter is observed. The primary diameter remains almost constant in the reactor working zone and the cooler because the rate of the surface reaction is diminished at the significantly lower reactant concentrations there. The final mean primary diameter is 277 nm.

Coagulation occurs throughout the reactor and cooler, as can be seen in the increasing collision diameter and decreasing particle number density, and the aggregate structure shown in the simulated TEMs, in Fig. 10. The final product consists of aggregates with a mean size of 2000 nm, comprised of on average 32 primary particles per particle, with a mean neck radius of 38 nm, indicating partial sintering between neighbouring connected primary particles.

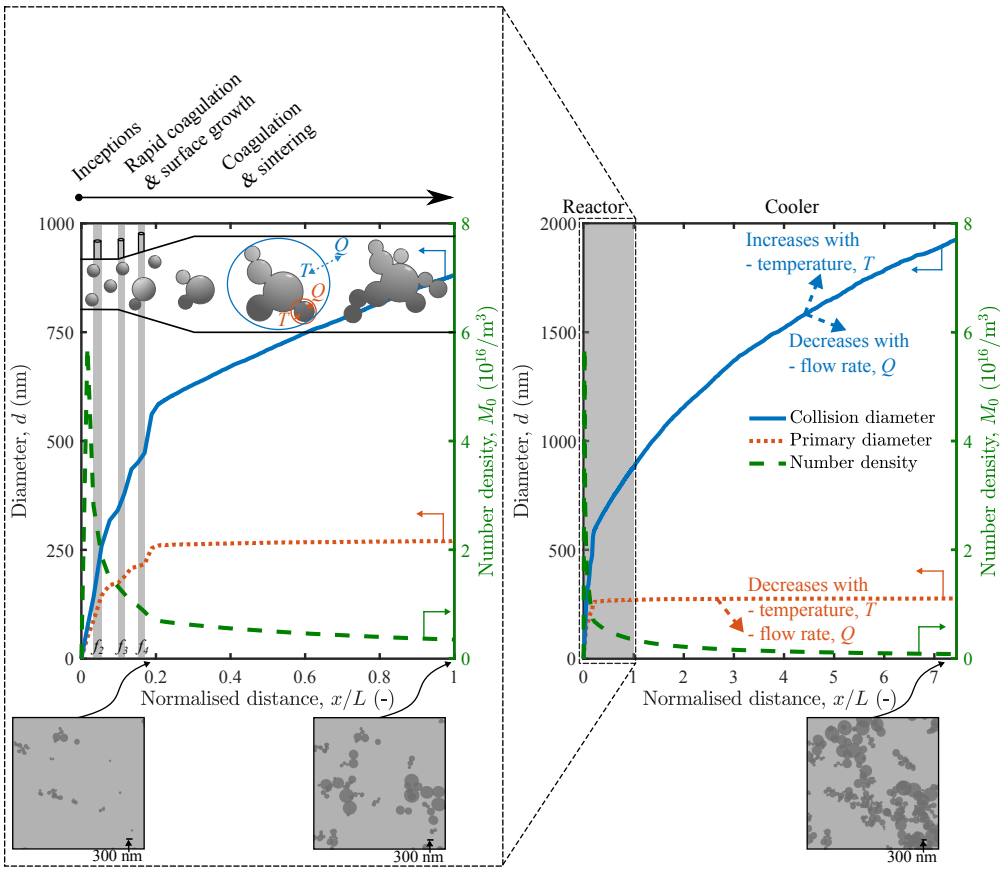

Fig. 10. Evolution of particle size and number density across the reactor and cooler (normalised by reactor length L) for the base conditions. Dashed arrows show the effects of increasing temperature T and throughput Q. The simulated TEM images were generated using the free-ware ray tracing program POV-Ray to visualise the simulation surface data for the set of computational particles.

Increasing the reactor temperature increased the mean collision diameter and decreased the mean primary diameter and number density. These trends are indicated with dashed arrows in Fig. 10 and can be explained by comparing the relative rates of the different processes at different temperatures. The particle process rates are greater at higher temperatures; however, the effect of temperature on the inception and coagulation rates is relatively large compared to the effect on the surface growth rate.

Akhtar et al. (1991) used an aerosol reactor to investigate the effect of temperature in the range 1200-1723 K. There, the PSD was found to shift to larger particle sizes with increased temperature and a theoretical study showed an increase in coagulation. As in the current work, there was little change in the geometric standard deviation (Table 3). Nakaso et al. (2003) also observed that, for temperatures in the range studied here, higher temperatures produced larger particles consisting of smaller primaries, and lower temperatures resulted in less dense aggregates of larger primaries. Other studies also report this effect (Zhou et al., 2006). The primary diameter might begin to increase again for temperatures higher than the ones investigated here due to complete sintering between primary particles (Nakaso et al., 2003).

Increasing the flow rate produced smaller primary and aggregate particles (indicated with dashed arrows in Fig. 10), and a higher number density because the particles had less time to grow. Again, this is supported by the trend reported in the literature (Akhtar et al., 1991) and this finding also agrees with empirical experience of the industrial process.

In this work, the same base case temperature profile was used for the early and late dosing cases. This is sufficient for the current study; however, the choice of dosing configuration is complex, since it affects the concentration profile and temperature exotherm. It would be useful to adjust the temperature profile to match the dosing strategy to account for the change in temperature due to the reaction. Here, the early dosing configuration created slightly smaller particles and a higher particle number concentration while the late dosing configuration produced significantly smaller primary particles (Table 3).

A smaller mean particle size is desirable to reduce milling requirements. This short study suggests that the use of high throughput, with rapid quenching at the end of the working zone and in the cooler, is necessary to minimise coagulation and sintering of the pigmentary particles and thereby improve product quality with minimal requirement on milling.

Table 3. Mean and geometric standard deviation (GSD, $\tilde{\sigma}$) of collision diameter and primary diameter and mean number density after the cooler for each case in Table 2.

Test case	Mean	GSD	Mean	GSD	Mean
-	$\bar{d}_{\mathrm{c}}$, nm	$\tilde{\sigma}_{d_{\mathrm{c}}}$	$\bar{d}_{\mathrm{p}}$, nm	$\tilde{\sigma}_{d_{\mathrm{p}}}$	$\bar{M}_0$, m^{-3}
Base case	2000	1.79	277	1.23	8.14×10^{14}
Early dosage	1910	1.77	272	1.21	8.44×10^{14}
Late dosage	1990	1.77	246	1.27	8.07×10^{14}
Low temperature	1800	1.74	356	1.23	9.02×10^{14}
High throughput	1590	1.76	251	1.23	15.1×10^{14}

5. Conclusions

This paper has presented a model for titania synthesis in an industrial reactor. Important features include an ideal reactor network to treat the flow behaviour and describe variations in composition and temperature; and a detailed population balance to describe the particle system, coupled to a comprehensive chemical mechanism. The use of a detailed particle model allows for many internal co-ordinates of the particles to be tracked, and these are believed to provide important information about the aggregate structure. Aggregate size and morphology are critical factors in determining the product quality, which in turn impacts the milling requirement of the industrial process. It is thus believed to be useful to obtain as much information as possible about the particle aggregates.

In particular, the distributions of the number of primary particles per particle, collision diameter, primary particle diameter, and neck radius are tracked

along the reactor-cooler. The pigmentary product leaving the cooler is shown to consist of partially sintered groups of connected primary particles, such that the particles are on average several times larger than their constituent primary particles. This has implications for the amount of milling that would be necessary to produce particles of the requisite size in the industrial process.

A preliminary sensitivity study found that increasing temperature resulted in the formation of larger particles, comprised of smaller primary particles, owing to the relative rates of the particle processes at different temperatures. This agrees with previous studies. Higher throughput produced smaller particles due to the limited time for reaction and particle growth. This is supported by empirical experience of the industrial process. Thus, although there is not currently industrial data to compare such trends quantitatively, the effects of operational changes were found to agree qualitatively with trends published for a number of laboratory studies.

This work serves as proof-of-concept for the use of a reactor network with a detailed population balance to simulate industrial titania synthesis. Avenues for future work could include development of a more detailed sintering model and inclusion of crystal structure information in the particle description. Regarding the latter, Xu et al. (2016) have recently demonstrated such a phase-transformation model in a CFD-population balance Monte Carlo simulation for flame synthesis of TiO_2. A full sensitivity study could then be performed towards optimising the PSD; investigating temperature hot-spots, the effect of the $AlCl_3$ additive (Shirley et al., 2009) and operational design limitations; and studying the parameters defining the particle processes. The Model Development Suite (MoDS) (CMCL Innovations, 2016) software tool could be utilised to do this, and to fit cheaper surrogate models (Forrester et al., 2008) to the simulation data.

Acknowledgements

This project is partly funded by the National Research Foundation (NRF), Prime Minister's Office, Singapore under its Campus for Research Excellence and Technological Enterprise (CREATE) programme. The authors would like to thank Huntsman Pigments and Additives for financial support.

Nomenclature

Upper-case Roman

A	Surface area	[m^2]
$\mathbf{C}$	Connectivity matrix	
E_a	Arrhenius activation energy	[$kJ \cdot mol^{-1}$]
K_{fm}	Free molecular regime coagulation kernel	
Kn	Knudsen number	
K_{sf}	Slip flow regime coagulation kernel	
K_{tr}	Transition regime coagulation kernel	
L	Length	[m]
M	Number of time steps	
M_0	0^{th} number moment	[m^{-3}]
M_k	k^{th} mass moment	[$kg^k \cdot m^{-3k}$]
N	Number of particles in the ensemble	
N_A	Avogadro's constant	[mol^{-1}]
P	Pressure	[bar]
$\mathbf{P}$	Probability	
P	Particle	
Q	System state	
R	Gas constant	[$m^3 \cdot bar \cdot K^{-1} \cdot mol^{-1}$]
R	Number of repeat runs	
T	Temperature	[K]
V	Volume	[m^3]
V_{smp}	Sample volume	[m^3]
W	Molecular weight	[$g \cdot mol^{-1}$]

Lower-case Roman

a_p	Primary particle area	[nm^2]
c	Confidence interval (here 99.9%)	
d_c	Collision diameter	[nm]
d_p	Primary particle diameter	[nm]
f	Volumetric feed fraction	
k_B	Boltzmann constant	[J·K^{-1}]
k_s	Surface growth rate constant, Arrhenius form	[m^4·s^{-1}·mol^{-1}]
k_1	Arrhenius constant	[m^4·s^{-1}·mol^{-1}]
m	Mass	[kg]
n	Number of primary particles	
p	Primary particle	
t	Time	[s]
v	Primary particle volume	[nm^3]
w	Statistical weight	
x	Axial distance	[m]

Lower-case Greek

$\bar{\epsilon}_\mathrm{stat}$	Average relative statistical error	
η	Number of elements	
θ	Property	
μ	Mean	
ρ	Mass/molar density (specified in the text)	[kg·m^{-3}]/[mol·m^{-3}]
σ	Standard deviation	
$\tilde{\sigma}$	Geometric standard deviation	
τ	Residence time	[s]
τ_c	Characteristic sintering time	[s]

Superscripts

max	Maximum
sph	Sphere (denotes a property of a mass equivalent sphere)

Subscripts

bc	Base case
i	Index variable
j	Index variable
k	Index variable
0	Denotes the number zero – added to the set of natural numbers

Symbols

$\mathbb{N}$	Set of natural numbers

Abbreviations

CFD	Computational fluid dynamics
CSTR	Continuous stirred tank reactor
DSA	Direct simulation algorithm
ERN	Equivalent reactor network
PFR	Plug flow reactor
PSD	Particle size distribution
SWA	Stochastic weighted algorithm
TEM	Transmission electron microscopy
MoDS	Model Development Suite

References

Akhtar, M.K., Lipscomb, G.G., Pratsinis, S.E., 1994. Monte Carlo Simulation of Particle Coagulation and Sintering. Aerosol Science and Technology 21, 83–93. doi:10.1080/02786829408959698.

Akhtar, M.K., Xiong, Y., Pratsinis, S.E., 1991. Vapor synthesis of titania powder by titanium tetrachloride oxidation. Journal of Aerosol Science 22, S35–S38. doi:10.1016/S0021-8502(05)80028-X.

Akroyd, J., Smith, A.J., Shirley, R., McGlashan, L.R., Kraft, M., 2011. A coupled CFD-population balance approach for nanoparticle synthesis in turbulent reacting flows. Chemical Engineering Science 66, 3792–3805. doi:10.1016/j.ces.2011.05.006.

Artelt, C., Schmid, H.J., Peukert, W., 2006. Modelling titania formation at typical industrial process conditions: effect of surface shielding and surface energy on relevant growth mechanisms. Chemical Engineering Science 61, 18–32. doi:10.1016/j.ces.2004.12.053.

Balthasar, M., Mauss, F., Knobel, A., Kraft, M., 2002. Detailed modeling of soot formation in a partially stirred plug flow reactor. Combustion and Flame 128, 395–409. doi:10.1016/S0010-2180(01)00344-3.

Celnik, M., Patterson, R.I.A., Kraft, M., Wagner, W., 2007. Coupling a stochastic soot population balance to gas-phase chemistry using operator splitting. Combustion and Flame 148, 158–176. doi:10.1016/j.combustflame.2006.10.007.

Chen, X., Mao, S.S., 2007. Titanium Dioxide Nanomaterials: Synthesis, Properties, Modifications, and Applications. Chemical Reviews 107, 2891–2959. doi:10.1021/cr0500535.

CMCL Innovations, 2016. MoDS (Model Development Suite). URL: http://www.cmclinnovations.com/mods/. Accessed: 2016-11-05.

Eibeck, A., Wagner, W., 2000. An Efficient Stochastic Algorithm for Studying Coagulation Dynamics and Gelation Phenomena. SIAM Journal on Scientific Computing 22, 802–821. doi:10.1137/S1064827599353488.

Eibeck, A., Wagner, W., 2001. Stochastic Particle Approximations for Smoluchoski's Coagualtion Equation. The Annals of Applied Probability 11, 1137–1165. doi:10.1214/aoap/1015345398.

Eibeck, A., Wagner, W., 2003. Stochastic interacting particle systems and nonlinear kinetic equations. The Annals of Applied Probability 13, 845–889. doi:10.1214/aoap/1060202829.

Forrester, A.I.J., Sóbester, A., Keane, A.J., 2008. Engineering Design via Surrogate Modelling: A Practical Guide. John Wiley & Sons, Chichester, UK. doi:10.1002/9780470770801.

Frenklach, M., Harris, S.J., 1987. Aerosol dynamics modeling using the method of moments. Journal of Colloid and Interface Science 118, 252–261. doi:10.1016/0021-9797(87)90454-1.

Garrick, S.C., Wang, G., 2011. Modeling and simulation of titanium dioxide nanoparticle synthesis with finite-rate sintering in planar jets. Journal of Nanoparticle Research 13, 973–984. doi:10.1007/s11051-010-0097-x.

Gázquez, M.J., Bolívar, J.P., Garcia-Tenorio, R., Vaca, F., 2014. A Review of the Production Cycle of Titanium Dioxide Pigment. Materials Sciences and Applications 05, 441–458. doi:10.4236/msa.2014.57048.

George, A.P., Murley, R.D., Place, E.R., 1973. Formation of TiO_2 aerosol from the combustion supported reaction of $TiCl_4$ and O_2. Faraday Symposia of the Chemical Society 7, 63. doi:10.1039/fs9730700063.

Ghoshtagore, R.N., 1970. Mechanism of Heterogeneous Deposition of Thin Film Rutile. Journal of The Electrochemical Society 117, 529. doi:10.1149/1.2407561.

Goudeli, E., Eggersdorfer, M.L., Pratsinis, S.E., 2015. Aggregate characteristics accounting for the evolving fractal-like structure during coagulation and sintering. Journal of Aerosol Science 89, 58–68. doi:10.1016/j.jaerosci.2015.06.008.

Hong, R., Ren, Z., Ding, J., Li, H., 2005. Experimental investigation and particle dynamic simulation for synthesizing titania nanoparticles using diffusion flame. Chemical Engineering Journal 108, 203–212. doi:10.1016/j.cej.2005.02.011.

Kartaev, E.V., Lukashov, V.P., Vashenko, S.P., Aulchenko, S.M., Kovalev, O.B., Sergachev, D.V., 2014. An Experimental Study of the Synthesis of Ultrafine Titania Powder in Plasmachemical Flow-Type Reactor. International Journal of Chemical Reactor Engineering 12, 377–396. doi:10.1515/ijcre-2014-0001.

Kartaev, V., Emelkin, V., Ktalkherman, M., Aulchenko, S., Vashenko, S., Kuzmin, V., 2015. Formation of counter flow jet resulting from impingement of multiple jets radially injected in a crossflow. Experimental Thermal and Fluid Science 68, 310–321. doi:10.1016/j.expthermflusci.2015.05.009.

Kobata, A., Kusakabe, K., Morooka, S., 1991. Growth and transformation of TiO_2 crystallites in aerosol reactor. AIChE Journal 37, 347–359. doi:10.1002/aic.690370305.

Koch, W., Friedlander, S., 1990. The effect of particle coalescence on the surface area of a coagulating aerosol. Journal of Colloid and Interface Science 140, 419–427. doi:10.1016/0021-9797(90)90362-R.

Kraft, M., 2005. Modelling of Particulate Processes. KONA Powder and Particle Journal 23, 18–35. doi:10.14356/kona.2005007.

Kruis, F.E., Kusters, K.A., Pratsinis, S.E., Scarlett, B., 1993. A Simple Model for the Evolution of the Characteristics of Aggregate Particles Undergoing

Coagulation and Sintering. Aerosol Science and Technology 19, 514–526. doi:10.1080/02786829308959656.

Lindberg, C., Akroyd, J., Kraft, M., 2016. On the milling behaviour of flame synthesised titania particles. Manuscript submitted for publication.

MathWorks, 2016. R2016a Documentation: 'ksdensity', Kernel smoothing function estimate for univariate and bivariate data. URL: https://www.mathworks.com/help/stats/ksdensity.html?searchHighlight=ksdensity. Accessed: 2016-11-09.

Mehta, M., Raman, V., Fox, R.O., 2013. On the role of gas-phase and surface chemistry in the production of titania nanoparticles in turbulent flames. Chemical Engineering Science 104, 1003–1018. doi:10.1016/j.ces.2013.10.039.

Mehta, M., Sung, Y., Raman, V., Fox, R.O., 2010. Multiscale Modeling of TiO_2 Nanoparticle Production in Flame Reactors: Effect of Chemical Mechanism. Industrial & Engineering Chemistry Research 49, 10663–10673. doi:10.1021/ie100560h.

Menz, W.J., Akroyd, J., Kraft, M., 2014. Stochastic solution of population balance equations for reactor networks. Journal of Computational Physics 256, 615–629. doi:10.1016/j.jcp.2013.09.021.

Menz, W.J., Kraft, M., 2013. The Suitability of Particle Models in Capturing Aggregate Structure and Polydispersity. Aerosol Science and Technology 47, 734–745. doi:10.1080/02786826.2013.788244.

Nakaso, K., Okuyama, K., Shimada, M., Pratsinis, S.E., 2003. Effect of reaction temperature on CVD-made TiO_2 primary particle diameter. Chemical Engineering Science 58, 3327–3335. doi:10.1016/S0009-2509(03)00213-6.

Novosselov, I.V., Malte, P.C., 2008. Development and Application of an Eight-Step Global Mechanism for CFD and CRN Simulations of Lean-Premixed

Combustors. Journal of Engineering for Gas Turbines and Power 130, 021502. doi:10.1115/1.2795787.

Novosselov, I.V., Malte, P.C., Yuan, S., Srinivasan, R., Lee, J.C.Y., 2006. Chemical Reactor Network Application to Emissions Prediction for Industial DLE Gas Turbine, in: Volume 1: Combustion and Fuels, Education, ASME. pp. 221–235. doi:10.1115/GT2006-90282.

Park, H.K., Park, K.Y., 2015. Control of Particle Morphology and Size in Vapor-Phase Synthesis of Titania, Silica and Alumina Nanoparticles. KONA Powder and Particle Journal 32, 85–101. doi:10.14356/kona.2015018.

Patterson, R.I.A., 2013. Convergence of Stochastic Particle Systems Undergoing Advection and Coagulation. Stochastic Analysis and Applications 31, 800–829. doi:10.1080/07362994.2013.817245.

Patterson, R.I.A., 2016. Properties of the solutions of delocalised coagulation and inception problems with outflow boundaries. Journal of Evolution Equations 16, 261–291. doi:10.1007/s00028-015-0302-6.

Patterson, R.I.A., Kraft, M., 2007. Models for the aggregate structure of soot particles. Combustion and Flame 151, 160–172. doi:10.1016/j.combustflame.2007.04.012.

Patterson, R.I.A., Singh, J., Balthasar, M., Kraft, M., Norris, J.R., 2006. The Linear Process Deferment Algorithm: A new technique for solving population balance equations. SIAM Journal on Scientific Computing 28, 303–320. doi:10.1137/040618953.

Patterson, R.I.A., Wagner, W., Kraft, M., 2011. Stochastic weighted particle methods for population balance equations. Journal of Computational Physics 230, 7456–7472. doi:10.1016/j.jcp.2011.06.011.

Pratsinis, S.E., Bai, H., Biswas, P., Frenklach, M., Mastrangelo, S.V.R., 1990. Kinetics of Titanium(IV) Chloride Oxidation. Journal of the American Ceramic Society 73, 2158–2162. doi:10.1111/j.1151-2916.1990.tb05295.x.

Pratsinis, S.E., Spicer, P.T., 1998. Competition between gas phase and surface oxidation of $TiCl_4$ during synthesis of TiO_2 particles. Chemical Engineering Science 53, 1861–1868. doi:10.1016/S0009-2509(98)00026-8.

Sander, M., West, R.H., Celnik, M.S., Kraft, M., 2009. A Detailed Model for the Sintering of Polydispersed Nanoparticle Agglomerates. Aerosol Science and Technology 43, 978–989. doi:10.1080/02786820903092416.

Shekar, S., Menz, W.J., Smith, A.J., Kraft, M., Wagner, W., 2012. On a multivariate population balance model to describe the structure and composition of silica nanoparticles. Computers & Chemical Engineering 43, 130–147. doi:10.1016/j.compchemeng.2012.04.010.

Shirley, R., Liu, Y., Totton, T.S., West, R.H., Kraft, M., 2009. First-Principles Thermochemistry for the Combustion of a $TiCl_4$ and $AlCl_3$ Mixture. The Journal of Physical Chemistry A 113, 13790–13796. doi:10.1021/jp905244w.

Spicer, P.T., Chaoul, O., Tsantilis, S., Pratsinis, S.E., 2002. Titania formation by $TiCl_4$ gas phase oxidation, surface growth and coagulation. Journal of Aerosol Science 33, 17–34. doi:10.1016/S0021-8502(01)00069-6.

Tsantilis, S., Kammler, H., Pratsinis, S., 2002. Population balance modeling of flame synthesis of titania nanoparticles. Chemical Engineering Science 57, 2139–2156. doi:10.1016/S0009-2509(02)00107-0.

Tsantilis, S., Pratsinis, S.E., 2000. Evolution of primary and aggregate particle-size distributions by coagulation and sintering. AIChE Journal 46, 407–415. doi:10.1002/aic.690460218.

Wells, C.G., 2006. A stochastic approximation scheme and convergence theorem for particle interactions with perfectly reflecting boundary conditions. Monte Carlo Methods and Applications 12, 291–342. doi:10.1515/156939606778705182.

West, R.H., Beran, G.J.O., Green, W.H., Kraft, M., 2007. First-Principles Thermochemistry for the Production of TiO_2 from $TiCl_4$. The Journal of Physical Chemistry A 111, 3560–3565. doi:10.1021/jp0661950.

West, R.H., Shirley, R.A., Kraft, M., Goldsmith, C.F., Green, W.H., 2009. A detailed kinetic model for combustion synthesis of titania from $TiCl_4$. Combustion and Flame 156, 1764–1770. doi:10.1016/j.combustflame.2009.04.011.

Xiong, Y., Pratsinis, S.E., 1991. Gas phase production of particles in reactive turbulent flows. Journal of Aerosol Science 22, 637–655. doi:10.1016/0021-8502(91)90017-C.

Xiong, Y., Pratsinis, S.E., 1993. Formation of agglomerate particles by coagulation and sintering – Part I. A two-dimensional solution of the population balance equation. Journal of Aerosol Science 24, 283–300. doi:10.1016/0021-8502(93)90003-R.

Xu, Z., Zhao, H., Zhao, H., 2016. CFD-population balance Monte Carlo simulation and numerical optimization for flame synthesis of TiO_2 nanoparticles. Proceedings of the Combustion Institute 000, 1–10. doi:10.1016/j.proci.2016.07.008.

Yapp, E.K., Patterson, R.I.A., Akroyd, J., Mosbach, S., Adkins, E.M., Houston Miller, J., Kraft, M., 2016. Numerical simulation and parametric sensitivity study of optical band gap in a laminar co-flow ethylene diffusion flame. Combustion and Flame 167, 320–334. doi:10.1016/j.combustflame.2016.01.033.

Zhou, E., Yuan, Z.F., Wang, Z., Fang, X.G., Gong, J.Z., 2006. Mechanism of scaling on oxidation reactor wall in TiO_2 synthesis by chloride process. Transactions of Nonferrous Metals Society of China 16, 426–431. doi:10.1016/S1003-6326(06)60073-3.

Appendix A. Particle size distributions

The probability density function of the collision diameter, $f(d_c)$, is estimated as the sum of log-normal distributions (for N stochastic particles in sample volume V_{smp}):

$$f(d_c) = \frac{1}{N} \sum_{n=1}^{N} \frac{1}{d_c \sigma \sqrt{2\pi}} \exp\left(- \frac{\left(\ln(d_c) - \ln\left(d_c^{(n)} \right) \right)^2}{2\sigma^2} \right). \tag{A.1}$$

Here, $d_c^{(n)}$ is the collision diameter of the n^{th} particle and σ is the standard deviation of the distribution, a parameter which can be modified to control the degree of smoothing. The number density is given by

$$g(d_c) = \frac{dn}{d(d_c)} = \frac{N}{V_{smp}} f(d_c) \tag{A.2}$$

and, from this,

$$\frac{dn}{d\ln(d_c)} = d_c \frac{dn}{d(d_c)} = d_c g(d_c). \tag{A.3}$$

Appendix B. Numerical Methods

Algorithm B.1: Reactor network algorithm with Strang operator-splitting scheme (Menz et al., 2014).

Input: Initial state Q_0 at t_0, final time t_f, time-step Δt, number of reactors n_{reac}
Output: Final state Q_f at t_f
Set $t \leftarrow t_0$, $Q \leftarrow Q_0$, $i_{reac} \leftarrow 1$
while $t < t_f$ **do**
  while $i_{reac} < n_{reac} + 1$ **do**
    Solve gas-phase chemistry for $\left[t, t + \frac{\Delta t}{2}\right]$.
    Solve particle-phase for $[t, t + \Delta t]$ using Algorithm B.2.
    Solve gas-phase chemistry for $\left[t + \frac{\Delta t}{2}, t + \Delta t\right]$.
    Increment $i_{reac} \leftarrow i_{reac} + 1$.
  end
  Increment $t \leftarrow t + \Delta t$.
end

Algorithm B.2: Direct simulation algorithm including particle inflow and outflow (Menz et al., 2014; Shekar et al., 2012)

Input: Initial state Q_0 at t_0, final time t_f

Output: Final state Q_f at t_f

Set $t \leftarrow t_0$, $Q \leftarrow Q_0$

while $t < t_f$ **do**

Generate an exponentially distributed waiting time τ with parameter:

$$R_{\text{total}}(Q) = R_{\text{inception}}(Q) + R_{\text{coagulation}}(Q) + R_{\text{surface}}(Q) + R_{\text{inflow}}(Q). \tag{B.1}$$

Choose process $\in$ {inception, surface, coagulation, inflow} by:

$$\mathbf{P}(\text{process}) = \frac{R_{\text{process}}(Q)}{R_{\text{total}}(Q)}. \tag{B.2}$$

if *process* = *inception* **then**

Perform inception by adding a new particle P_{N+1} to the ensemble.

else if *process* = *coagulation* **then**

Uniformly select two particles P_i, P_j, perform any tagged deferred events and then perform successful coagulation with probability:

$$\mathbf{P}_{i,j} = \frac{K_{\text{tr}}(P_i, P_j)}{\hat{K}(P_i, P_j)} \tag{B.3}$$

where $\hat{K}$ is the majorant kernel.

else if *process* = *surface* **then**

Uniformly select a particle P_i and, from this, a primary particle p_j.

if *defer* = *true* **then**

Tag p_j for deferred surface reaction.

else

Perform surface reaction on p_j.

end

else if *process* = *inflow* **then**

Uniformly select a particle P_i and add N_{in} copies to the ensemble.

$$N_{\text{in}} = \frac{V_{\text{smp}}}{V_{\text{smp}}^{(j)}} \tag{B.4}$$

V_{smp} and $V_{\text{smp}}^{(j)}$ in Eq. (B.4) are the current and inflow scaling factors.

end

Perform continuous outflow and sintering for $[t, t+\tau]$ and rescale the sample volume (τ_{CSTR} is the reactor residence time):

$$V_{\text{smp}}^{\text{new}} = \frac{V_{\text{smp}}}{1 - \tau/\tau_{\text{CSTR}}}. \tag{B.5}$$

Increment $t \leftarrow t + \tau$.

end

Perform outstanding deferred processes.